Supplementary material for: Continuum Simulations of Water Flow in Carbon Nanotube Membranes

A. Popadić

Laboratory for Molecular Modeling, National Institute of Chemistry, Hajdrihova 19, SI-1001 Ljubljana, Slovenia

J. H. Walther

Department of Mechanical Engineering, Technical University of Denmark, DK-2800 Kgs. Lyngby, Denmark.
Also at: Chair of Computational Science, ETH Zurich, Clausiusstrasse 33, CH-8092 Zurich, Switzerland

E-mail: jhw@mek.dtu.dk

P. Koumoutsakos

Chair of Computational Science, ETH Zurich, Clausiusstrasse 33, CH-8092 Zurich, Switzerland

E-mail: petros@ethz.ch

M. Praprotnik

Laboratory for Molecular Modeling, National Institute of Chemistry, Hajdrihova 19, SI-1001 Ljubljana, Slovenia

E-mail: praprot@cmm.ki.si

1. Partial-slip boundary condition

For the partial-slip boundary condition we allow a nonzero tangential component of flow velocity at the wall. For the normal component, on the other hand, we demand to vanish at the wall. We use the Navier boundary condition, which assumes a linear dependence of shear stress on the tangential component of flow velocity at the wall [1]. Stress tensor at the wall thus reads as

$$\sigma_{ik} n_k = \lambda v_{ti} - p' n_i, \tag{1}$$

where n_k is the k-th cartesian component of the normal to the wall with the normal pointing into the fluid. λ is the friction coefficient between the wall and the fluid and p' is the total pressure exerted on the wall by the fluid. The stress tensor of the bulk liquid reads as

$$\sigma_{ik} = \mu \left(\frac{\partial v_i}{\partial x_k} + \frac{\partial v_k}{\partial x_i} \right) - p\delta_{ik}, \tag{2}$$

where μ is the viscosity of the liquid and p the hydrodynamic pressure [2]. By requiring the balance of stress at the fluid-solid interface we obtain the velocity boundary condition

$$\lambda \mathbf{v}_t - p'\mathbf{n} = \mu[2(\mathbf{n}\cdot\nabla)\mathbf{v} + \mathbf{n}\times(\nabla\times\mathbf{v})] - p\mathbf{n}. \tag{3}$$

This boundary condition can be divided into a tangential and a normal component

$$\mathbf{v}_t \cdot \mathbf{n} = 0, \tag{4}$$

$$\mathbf{v}_n = (\mathbf{v}\cdot\mathbf{n})\mathbf{n}. \tag{5}$$

The tangential component reads as

$$\mathbf{v}_t = \frac{\mu}{\lambda}[2(\mathbf{n}\cdot\nabla)\mathbf{v}_t + \mathbf{n}\times(\nabla\times\mathbf{v_t}) + \mathbf{n}\times(\nabla\times\mathbf{v_n})]. \tag{6}$$

The curl of the normal component of velocity is zero by Stokes theorem and thus the last term in brackets is zero. Using the following relation

$$\nabla(\mathbf{a}\cdot\mathbf{b}) = (\mathbf{a}\cdot\nabla)\mathbf{b} + (\mathbf{b}\cdot\nabla)\mathbf{a} + \mathbf{a}\times(\nabla\times\mathbf{b}) + \mathbf{b}\times(\nabla\times\mathbf{a}). \tag{7}$$

to rewrite the second term in Eq. (6) and realizing that the curl of the normal is again zero by Stokes theorem we obtain the partial-slip boundary condition

$$\mathbf{v}_t = \frac{\mu}{\lambda}[(\mathbf{n}\cdot\nabla)\mathbf{v}_t - (\mathbf{v}_t\cdot\nabla)\mathbf{n}]. \tag{8}$$

The first term on RHS is the gradient of the tangential component of velocity in the direction normal to the wall and the second term is the curvature of the wall in the flow direction. This enables us to write the boundary condition in a more compact form

$$v_t = l_s \left[\frac{\partial v_t}{\partial n} - \frac{v_t}{r} \right], \tag{9}$$

where r is the radius of the curvature of the wall in the flow direction‡ with the curvature being negative for concave boundaries. We introduce the slip length $l_s = \mu/\lambda$, which

‡ This curvature should not be mistaken for the curvature of the diameter of the nanotube. Thus the second term in Eq. (9) is not required for a cylindrical nanotube in periodic boundary conditions or an infinitely long tube.

for non-curved boundaries gives the depth at which the linear extrapolation of the flow velocity profile into the wall reaches zero [1]. A vanishing slip length $l_s = 0$ nm corresponds to the standard no-slip boundary condition where the fluid velocity vanishes at the boundary. A diverging slip length $l_s \to \infty$ corresponds to a full-slip boundary condition with no friction between the fluid and the wall at the interface. The boundary condition Eq. 9 then reads

$$\frac{\partial v_t}{\partial n} = \frac{v_t}{r}. \tag{10}$$

By taking the normal component of Eq. (3) we obtain the total pressure exerted on the wall

$$p' = p - 2\mu \frac{\partial v_n}{\partial n}. \tag{11}$$

The partial-slip boundary condition in Eq. (9) differs from the more intuitive and frequently used form of the Navier boundary condition [3, 4, 5, 6]

$$v_t = \tilde{l}_s \frac{\partial v_t}{\partial n} \tag{12}$$

by the additional term depending on the wall curvature. This leads to a different definition of the slip length, i.e. $\tilde{l}_s$ instead of l_s. The absence of the curvature term in the boundary condition can result in a significant dependence of slip length $\tilde{l}_s$ on the shape of the boundary [7]. Einzel et al. discussed the dependence of $\tilde{l}_s$ from the boundary shape [8]. They express the slip length $\tilde{l}_s$ for a curved boundary with the slip length $\tilde{l}_{s0}$ for a flat boundary and the curvature of the boundary

$$\frac{1}{\tilde{l}_s} = \frac{1}{\tilde{l}_{s0}} + \frac{1}{r} = \frac{1}{l_s} + \frac{1}{r}. \tag{13}$$

By $r \to \infty$ we recognise that l_s and $\tilde{l}_s$ are the same for the flat boundary. The slip length l_s is the ratio of the liquid viscosity and the friction coefficient between the liquid and the solid, both positive quantities. Consequentially the slip length l_s is also a positive quantity, whereas $\tilde{l}_s$ can be negative for $-l_s < r < 0$ [7]. Furthermore, a diverging slip length l_s results in a vanishing shear stress at the boundary. Applying such a boundary condition to a problem of a steady Stokes flow past a sphere results in the proper force to the sphere with the full-slip boundary condition [9]

$$\mathbf{F} = 4\pi\mu R\mathbf{V}_0, \tag{14}$$

where $\mathbf{V}_0$ is the fluid velocity far from the sphere. A diverging $\tilde{l}_s$, however, results in a nonvanishing shear stress at the boundary

$$\sigma_{\text{shear}} = -\mu \frac{v_t}{r}. \tag{15}$$

To achieve a vanishing stress at the boundary a negative slip length $\tilde{l}_s$ is needed with $\tilde{l}_s = -r$.

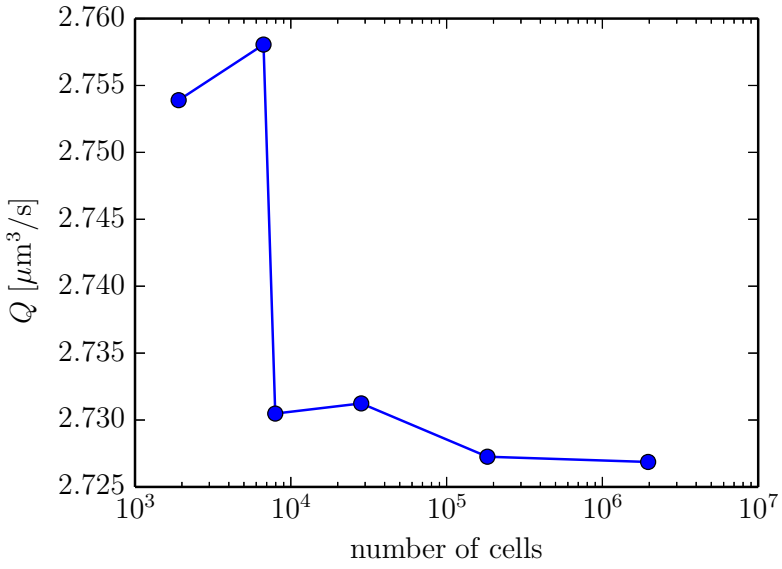

Figure 1. Mesh independence test on a 20 nm section of an infinite CNT of radius 1 nm with the no-slip boundary condition imposed at the walls. The pressure drop between the ends of the section of the CNT is 10^8 Pa.

2. Computational details

2.1. Mesh independence

To check mesh independence we first simulate a water flow through an infinite CNT and as in our study of the CNT membrane [10] we consider only one quarter of the CNT by imposing symmetry plane boundary conditions. We prepare a 20 nm section of an infinite CNT of radius $R = 1$ nm. At the ends of the CNT section we impose periodic boundaries with a pressure drop of 10^8 Pa and measure the volumetric flow through the CNT. The study of mesh independence on this system (Fig. 1) yields the accuracy requirements for mesh building inside the CNT of our CNT membrane system. This simple system, because an analytic solution is known, also provides the opportunity to check our partial-slip boundary condition implementation (Fig. 2). We then check mesh independence on our CNT membrane system [10]. We test mesh independence on a CNT of length $L^* = 19.5$, the radius of curvature of the fillet $r_f^* = 0.3$ and the Reynolds number $\mathrm{Re} = 1.4 \times 10^{-3}$ for the full-slip and no-slip boundary conditions.

2.2. Solution convergence

We run simulations until the residuals drop below 10^{-6} (Fig. 4). For reference we give the convergence of pressure loss between the inlet and the outlet for different boundary conditions (Fig. 5).

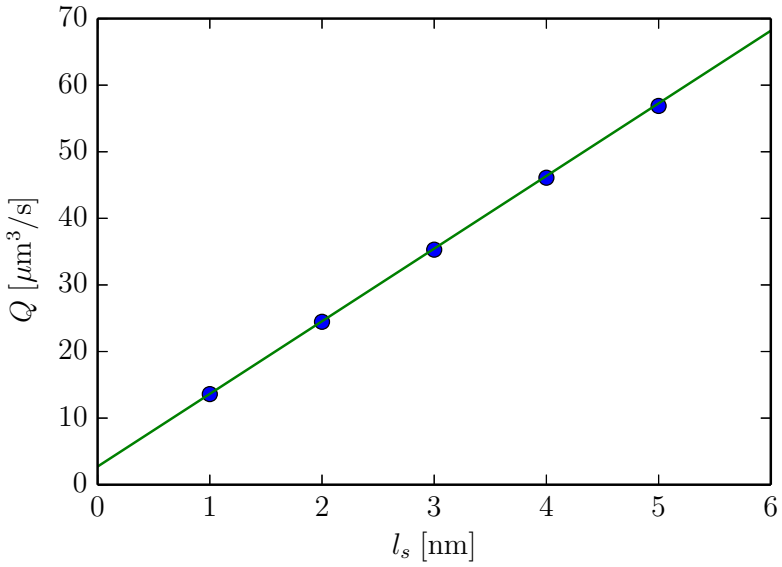

Figure 2. Volumetric flow rate through a 20 nm section of an infinite CNT of radius 1 nm with a constant pressure gradient of 5×10^{15} Pa/m. The blue dots are the volumetric flow rates obtained with CFD and the green line represents the analytically obtained volumetric flow rate.

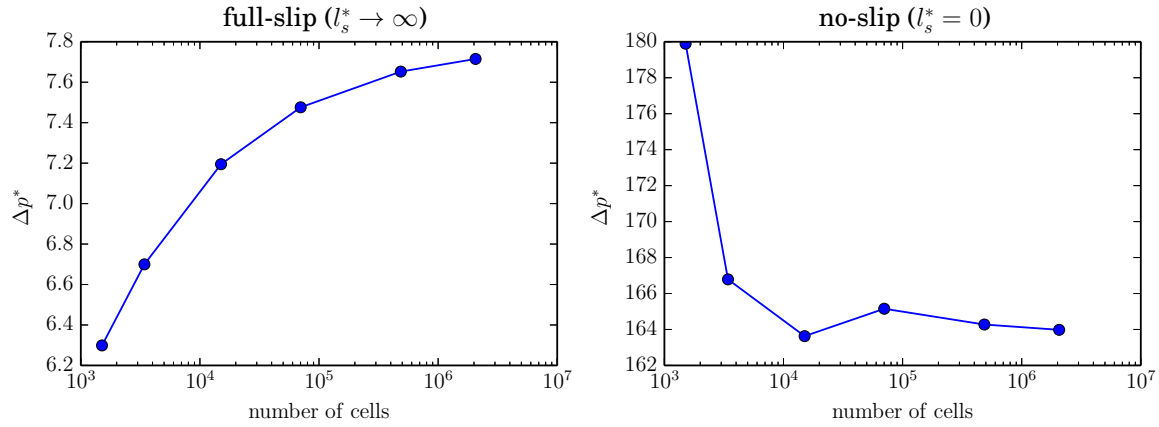

Figure 3. Mesh independence test on a CNT with $L^* = 19.5$, $r_f = 0.3$ and $\mathrm{Re} = 1.4 \times 10^{-3}$ for the full-slip and the no-slip boundary conditions.

3. Visiualization of the flow field at the CNT ends

Fig. 6 shows the fluid motion in the vicinity of the CNT entrance with a rounded corner by a fillet with the radius of curvature $r_f^* = 0.3$ and the Reynolds number $\mathrm{Re} = 1.4 \times 10^{-3}$. We show fluid flow for three different boundary conditions: the full-slip, the partial-slip with $l_s^* = 1/6$, and the no-slip boundary condition. We observe that the boundary condition does not strongly affect the direction of the fluid motion. It does, however, affect the velocity magnitude profile. We also show the vorticity in

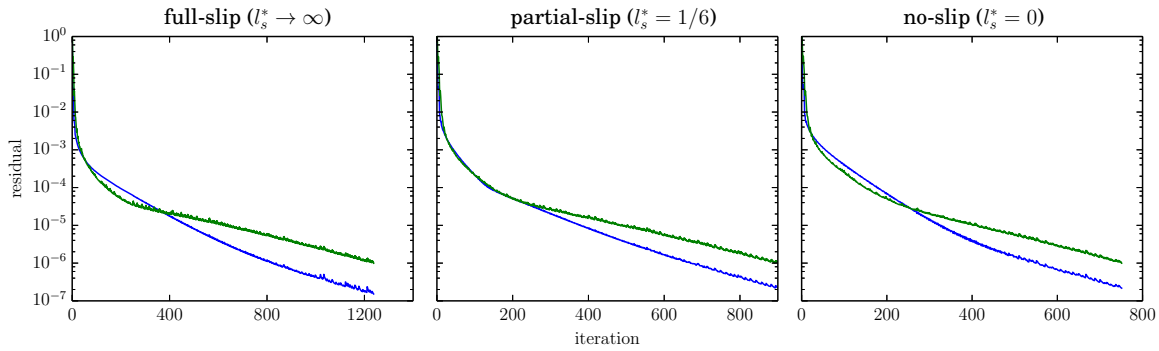

Figure 4. Residual convergence for a CNT of length $L^* = 29.5$ with the radius of the curvature of the fillet $r_f^* = 0.3$ and the Reynolds number $\mathrm{Re} = 1.4 \times 10^{-3}$ for three different boundary conditions: a full-slip boundary condition, a partial-slip boundary condition with $l_s^* = 1/6$ and a no-slip boundary condition. The blue curve represents the momentum residuals and the green curve the mass residuals.

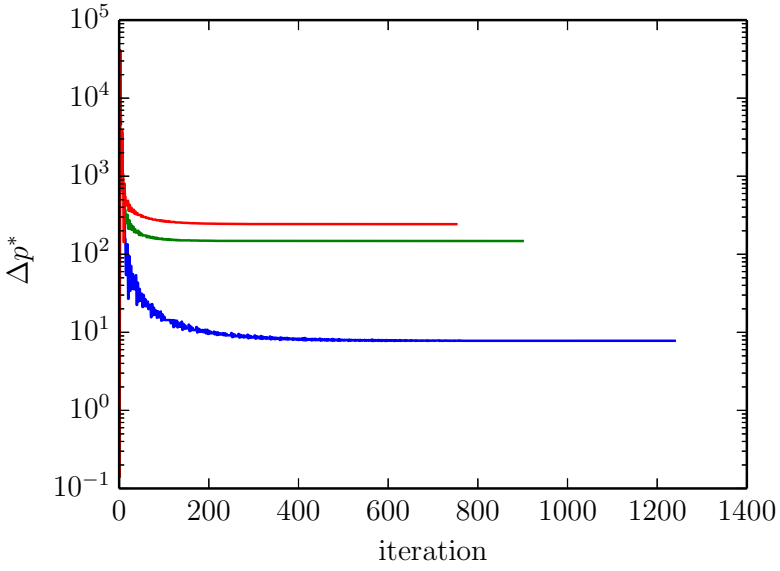

Figure 5. Convergence of pressure loss between the inlet and the outlet of a CNT of length $L^* = 29.5$ with the radius of the curvature of the fillet 0.3 nm and the Reynolds number $\mathrm{Re} = 1.4 \times 10^{-3}$ for three different boundary conditions: a full-slip boundary condition (blue), a partial-slip boundary condition with $l_s^* = 1/6$ (green) and a no-slip boundary condition (red).

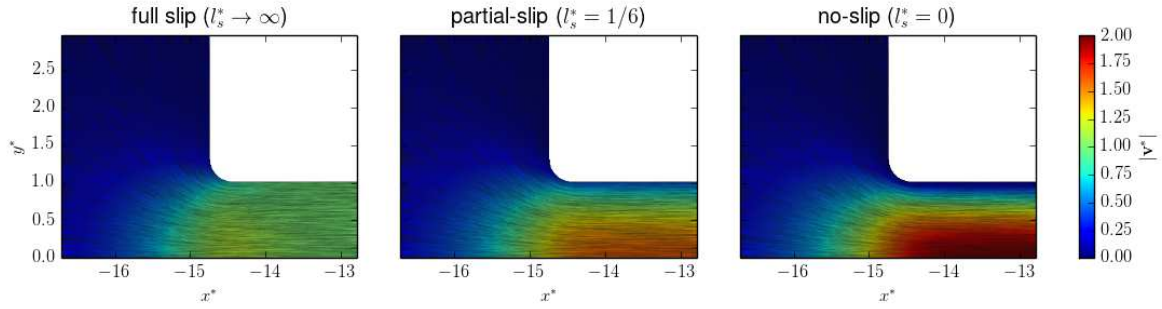

Figure 6. Line integral convolution of the fluid velocity on top of the fluid velocity magnitude profile showing the fluid motion for three different boundary conditions: the full-slip boundary condition, the partial-slip boundary condition with $l_s^* = 1/6$ and the no-slip boundary condition. The radius of the curvature of the fillet is $r_f^* = 0.3$ and the Reynolds number is $\mathrm{Re} = 1.4 \times 10^{-3}$.

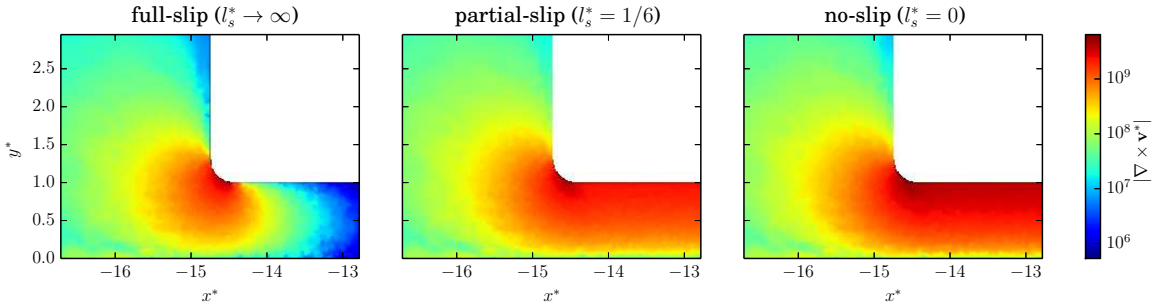

Figure 7. Nondimensional vorticity magnitude in the vicinity of the CNT entrance for three different boundary conditions: the full-slip boundary condition, the partial-slip boundary condition with $l_s^* = 1/6$ and the no-slip boundary condition. The radius of the curvature of the fillet is $r_f^* = 0.3$ and the Reynolds number is $\mathrm{Re} = 1.4 \times 10^{-3}$.

the vicinity of the CNT entrance in Fig. 7 for all three cases. All three cases, regardless of the boundary condition, exhibit an increased vorticity at the CNT entrance due to contraction of the flow streamlines into the small CNT opening.

Fig. 8 depicts the velocity profile for the flow through a thin orifice and the slip enhanced Hagen-Poiseuille flow. The figure clearly shows the similarity between the velocity profile of the flow through a thin orifice and the slip enhanced Hagen-Poiseuille flow with $l_s^* = 1/6$. Due to this similarity the viscous energy dissipation at the CNT ends has its minimum for $l_s^* = 1/6$.

4. Boundary condition at outer walls

We check the effect of the boundary condition at the outer walls of the CNT membrane. Again we impose three different boundary conditions at the outer walls of the CNT membrane: the full-slip, the partial-slip with l_s^* at the outer wall equal to l_s^* inside the CNT, and the no-slip boundary condition. With these boundary conditions we measure

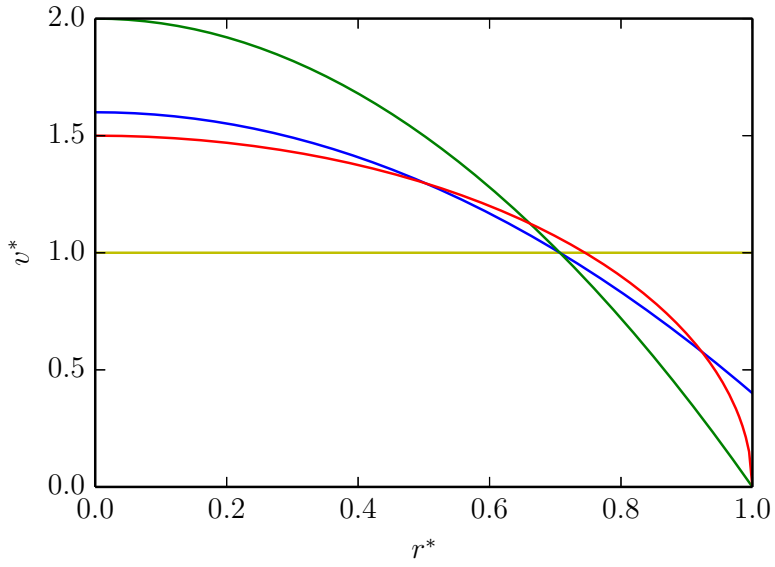

Figure 8. Velocity profile of the flow through a thin orifice (red) and the slip enhanced Hagen-Poiseuille flow for the full-slip boundary condition (orange), the partial-slip boundary condition with $l_s^* = 1/6$ (blue) and the no-slip boundary condition (green).

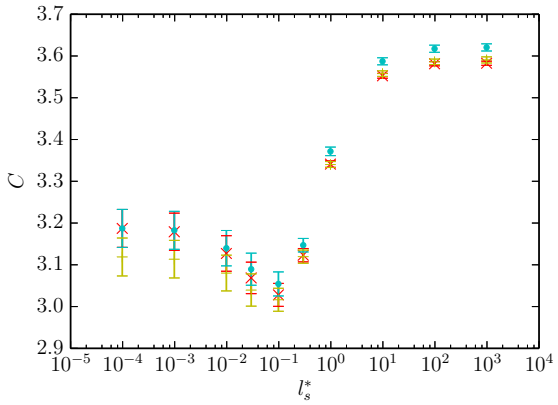

Figure 9. Pressure loss at the CNT ends dependence form l_s^* for different boundary conditions at the outer wall of the CNT membrane: the full-slip boundary condition (orange), the partial slip boundary condition with l_s^* at the outer wall equal to l_s^* inside the CNT (red) and the no-slip boundary condition (light blue). The radius of the curvature of the fillet is $r_f^* = 0$ and the Reynolds number is $\mathrm{Re} = 1.4 \times 10^{-3}$.

pressure losses at the CNT ends (Fig. 9) and conclude that the boundary condition at the outer walls of the CNT membrane has negligible effect. This is in agreement with Gravelle et. al. who also found the boundary condition at the outer walls to have negligible impact [11].

References

[1] Bocquet L and Charlaix E 2010 *Chem. Soc. Rev.* **39** 1073–1095
[2] Landau L D and Lifshitz E M 1987 *Fluid Mechanics* 2nd ed (*Course of Theoretical Physics* vol 6) (Butterworth-Heinemann)
[3] Morris D L, Hannon L and Garcia A L 1992 *Phys. Rev. A* **46** 5279–5281
[4] Bocquet L and Barrat J L 2007 *Soft Matter* **3** 685–693
[5] Thomas J A and McGaughey A J H 2008 *Nano Lett.* **8** 2788–2793
[6] Erbaş A, Podgornik R and Netz R R 2010 *Eur. Phys. J. E.* **32** 147–164
[7] Walther J H, Werder T, Jaffe R L and Koumoutsakos P 2004 *Phys. Rev. E* **69** 062201
[8] Einzel D, Panzer P and Liu M 1990 *Phys. Rev. Lett.* **64** 2269–2272
[9] Padmavathi B S, Amaranath T and Nigam S D 1993 *Fluid Dyn. Res.* **11** 229–234
[10] Popadić A, Walther J H, Koumoutsakos P and Praprotnik M Original paper
[11] Gravelle S, Joly L, Detcheverry F, Ybert C, Cottin-Bizonne C and Bocquet L 2013 *PNAS* **110** 16367–16372